



Full-state autopilot-guidance design under a linear quadratic differential game formulation

M. Levy ^{*}, T. Shima, S. Gutman

Technion - Israel Institute of Technology, Israel



ARTICLE INFO

Keywords:

Guidance systems
Linear optimal control
Game theory

ABSTRACT

Full-state single-loop and full-state two-loop autopilot-guidance architectures are derived under a linear quadratic differential game formulation. In the full-state single-loop case, the guidance command is injected directly to the actuator, whereas in the full-state two-loop case, it is the input to the autopilot loop. To prevent impractical end-game scenarios, where the states diverge to unacceptable values, a cost function that includes appropriate running cost terms on some of the states is proposed. The conditions for obtaining an equivalence relation between the full-state single-loop and full-state two-loop architectures are derived under a linear quadratic differential game formulation and the proposed cost function. Under such a formulation, the two full-state architectures are identical if and only if the number of guidance commands matches the number of available controllers. The guidance laws performance is illustrated using an interceptor missile having forward and aft controls in linear and nonlinear settings, while considering two types of evasion strategies. The first strategy is a linear controller based on the linear quadratic differential game solution. The second strategy is a “bang–bang” controller based on the optimal evasion solution. It is shown that the linear evasion strategy may not be suitable to represent a realistic evading strategy. In addition, the conditions for the existence of a saddle point solution are analyzed for the two full-state guidance laws.

1. Introduction

The term full-state guidance law refers to an autopilot-guidance system that has a full-state feedback into the guidance loop, and thus the coupling between the guidance and flight-control (G&C) loops is taken into account. Such a design may enhance the interceptor’s performance and has the potential to meet advanced design requirements, i.e. improved accuracy and extended kill envelope. Two types of full-state G&C architectures were considered in previous papers (Idan, Shima, & Golan, 2007; Levy, Shima, & Gutman, 2013, 2015, 2017; Menon & Ohlmeyer, 2001; Menon, Sweriduk, & Ohlmeyer, 2003; Palumbo, Reardon, & Blauwkamp, 2004; Rusnak & Levi, 1991; Shima, Idan, & Golan, 2006; Shkolnikov, Shtessel, & Lianos, 2001): full-state single-loop (FS-SL) and full-state two-loop (FS-TL). In the FS-TL case, the inner autopilot loop is designed independently of the outer guidance one, whereas in the FS-SL case, the guidance command is injected directly to the actuator, without a definite autopilot.

In the literature, the term “integrated guidance law” has been used to describe full-state G&C systems. In Palumbo et al. (2004), Shima et al. (2006), Idan et al. (2007), Menon and Ohlmeyer (2001) and Menon et al. (2003), the term “integrated” referred to FS-SL guidance systems,

whereas in Shkolnikov et al. (2001) the term referred to an FS-TL autopilot-guidance system. The general solution of an optimal guidance law with a full-state feedback was derived for an arbitrary order autopilot model in Rusnak and Levi (1991). Theoretical results concerning the equivalence of the two full-state architectures were presented under one-sided optimal control formulation for linear quadratic optimization problems (Levy et al., 2013, 2015) and for nonlinear optimization problems with bounded controls (Levy et al., 2017).

In practice, the controller is bounded, which results in a nonlinear system during saturation. In fact, during saturation the G&C loop is opened and if in addition the open loop transfer function is unstable or close to instability, the attitude angle may diverge to unacceptable values (Gutman, Rubinsky, Shima, & Levy, 2013). In the nonlinear approach, the states can be kept at reasonable values by limiting the commands and using a carefully designed autopilot. In the linear quadratic approach, this can be done indirectly by adding running cost terms of each of the controllers to the cost function.

Perfect information of the target future maneuver is usually not available. Hence, an appropriate alternative to the optimal control formulation is the zero-sum pursuit-evasion game formulation (Isaacs,

^{*} Corresponding author.

E-mail address: maital.le@alumni.technion.ac.il (M. Levy).

1965), where only the information on the target maneuver capability is required. The linear quadratic differential game (LQDG) formulation was presented in Ho, Bryson, and Baron (1965) while assuming ideal dynamics for both adversaries. In Ben-Asher and Yaesh (1998), this assumption was replaced by first-order dynamics for both the missile and the target. In Ben-Asher, Levinson, Shinar, and Weiss (2004) it was shown that an inclusion of a running cost on the state variables in LQDG guidance laws has a disturbance attenuation effect. In Turetsky and Shinar (2003), the bounded-control and LQDG formulations were compared by assuming first-order dynamics for both players.

In the present paper, FS-SL and FS-TL autopilot-guidance laws are derived under an LQDG formulation, by assuming: linear dynamics for both adversaries, perfect information of the states, and unbounded controls. The equivalence condition of the two full-state guidance laws is provided for a cost function that contains running cost terms of the states. According to the theorem, the two full-state optimization problems are identical if and only if the number of guidance commands is identical to the number of available controllers. This result encourages usage of the FS-TL architecture over the FS-SL one in practical autopilot-guidance systems. In these systems the autopilot is an important component since it ensures the inner stability of the airframe if the guidance loop is inactive. Thus, by following the equivalence condition, the FS-TL architecture can have the best of both worlds: inner stable autopilot loop, and at the same time, the same cost as the FS-SL architecture.

Preliminary results related to the present work appeared in Levy, Shima, and Gutman (2014). The present paper expands on Levy et al. (2014) in several directions:

1. The conditions for the existence of a saddle point solution are analyzed for both FS-SL and FS-TL architectures.
2. Derivation of the optimal evasion strategy in a practical bounded control setting against an LQDG maneuvering missile.
3. A thorough analysis of the FS-SL and FS-TL performance is done using linear and nonlinear test scenarios, while considering two types of target acceleration commands. The first evasion strategy is linear and is based on the LQDG formulation. The second evasion strategy is of “bang–bang” type and is based on the optimal evasion solution against an LQDG guided missile.

The remainder of this paper is organized as follows. The linearized model derivation and autopilot-guidance design are given in Section 2 and Section 3, respectively. The equivalence of the two full-state guidance laws is presented in Section 4. The test case and the corresponding guidance laws formulations are given in Section 5 and Section 6, respectively. Simulation results were made for two types of target strategies: an LQDG one and the optimal evasion strategy against an LQDG guided missile. These strategies are presented in Section 7, followed by the simulation results in Section 8, and the concluding remarks. The nonlinear models of the relative kinematics and missile lateral dynamics are presented in Appendix.

2. Linearized model derivation

This section provides the design assumptions and describes the linearized end-game geometry used for the synthesis of the guidance laws and their analysis.

2.1. Design assumptions

The derivation of the guidance laws will be performed based on the following assumptions:

1. A skid-to-turn roll-stabilized missile is considered. The motion of such a missile can be separated into two perpendicular channels, thus allowing to treat only a planar motion.
2. Linear dynamics for the target and the missile.

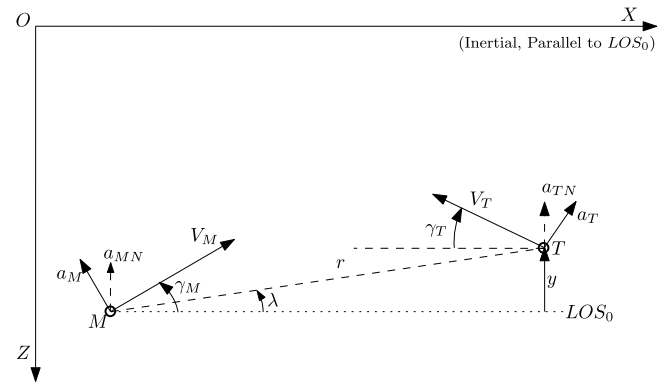


Fig. 1. Planar engagement geometry.

3. The missile and target deviations from the collision triangle are small during the end-game, consequently the relative end-game trajectory can be linearized about the nominal line of sight (LOS).
4. Constant speeds are assumed for both the missile and the target.

2.2. End-game scenario description

Fig. 1 presents a schematic view of the planar end-game geometry, where X axis is aligned with the initial LOS (LOS_0) and Z axis is perpendicular to it. The subscripts M and T denote the missile and the target, respectively. V , a , and γ denote the speed, normal acceleration, and path angle. a_{MN} , and a_{TN} are respectively the missile and target accelerations normal to LOS_0 . r is the range between the adversaries and λ is the angle between the LOS and the X axis. y is the relative displacement between the target and the missile normal to the X axis.

The missile and the target accelerations normal to the initial LOS are

$$a_{MN} \approx a_M \cos(\gamma_{M0}), \quad a_{TN} \approx a_T \cos(\gamma_{T0}) \quad (1)$$

Then, the corresponding kinematic equation is

$$\dot{y} = a_{TN} - a_{MN} \quad (2)$$

2.3. Linear equations of motion

The general set of equations can be classified into three categories: kinematics equations, dynamics equations, and servo model equations. Thus, the general state vector is given by

$$\mathbf{x} = \begin{bmatrix} \mathbf{x}_K \\ \mathbf{x}_D \\ \mathbf{x}_S \end{bmatrix} \quad (3)$$

where $\mathbf{x}_K \in \mathbb{R}^{n_K \times 1}$ denotes the kinematics states, e.g. the missile-target separation; $\mathbf{x}_D \in \mathbb{R}^{n_D \times 1}$ denotes the dynamics states, e.g. the missile's angular rates; $\mathbf{x}_S \in \mathbb{R}^{n_S \times 1}$ denotes the servo model states.¹

The target dynamics is assumed to be ideal to consider a realistic scenario where there is no information on its dynamics. In this manner, by assuming ideal target dynamics, the worst-case scenario is taken into account. Let $v \in \mathbb{R}^1$ denote the target controller, then

$$a_{TN} = v \quad (4)$$

The dynamics and servo equations of the missile are given as follows

$$\begin{bmatrix} \dot{\mathbf{x}}_D \\ - \\ \dot{\mathbf{x}}_S \end{bmatrix} = \begin{bmatrix} \mathbf{A}_D \\ \mathbf{0} \end{bmatrix} \begin{bmatrix} \mathbf{x}_D \\ \mathbf{x}_S \end{bmatrix} + \begin{bmatrix} \mathbf{0} \\ \mathbf{B}_S \end{bmatrix} \mathbf{u}_S \quad (5)$$

¹ The equations of motions take into account the servo dynamics.

where $\mathbf{u}_S \in \mathbb{R}^{m_S \times 1}$ is the servo command, and $[0]$ is a matrix of zeros with appropriate dimensions. The matrix \mathbf{A}_D in Eq. (5) may be rewritten as follows

$$\mathbf{A}_D = \begin{bmatrix} \mathbf{A}_{DD} & \mathbf{A}_{DS} \end{bmatrix} \quad (6)$$

where $\mathbf{A}_{DD} \in \mathbb{R}^{n_D \times n_D}$ and $\mathbf{A}_{DS} \in \mathbb{R}^{n_D \times n_S}$.

Denote the combined dynamics and servo state vector by $\mathbf{x}_{DS} \in \mathbb{R}^{(n_D+n_S) \times 1}$, then the general form of the missile's normal acceleration is

$$a_{MN} = \mathbf{C}_M \mathbf{x}_{DS}, \quad \mathbf{x}_{DS} \triangleq \begin{bmatrix} \mathbf{x}_D \\ \mathbf{x}_S \end{bmatrix} \quad (7)$$

Substituting Eq. (7) into the kinematics equation (Eq. (2)) and combining with Eq. (4), the set of kinematics equations is obtained

$$\dot{\mathbf{x}}_K = \begin{bmatrix} \mathbf{A}_{KK} & \mathbf{A}_{K,DS} \end{bmatrix} \begin{bmatrix} \mathbf{x}_K \\ \mathbf{x}_{DS} \end{bmatrix} + \mathbf{C}_K v, \quad \mathbf{x}_K = [y \quad \dot{y}]^T \quad (8)$$

where

$$\mathbf{A}_{KK} = \begin{bmatrix} 0 & 1 \\ 0 & 0 \end{bmatrix}, \quad \mathbf{A}_{K,DS} = \begin{bmatrix} [0] \\ -\mathbf{C}_M \end{bmatrix}, \quad \mathbf{C}_K = \begin{bmatrix} 0 \\ 1 \end{bmatrix} \quad (9)$$

The general set of equations is obtained by combining the dynamics-servo equations (Eq. (5)) and the kinematics equations (Eq. (8))

$$\dot{\mathbf{x}} = \mathbf{A} \mathbf{x} + \mathbf{B} \mathbf{u}_S + \mathbf{C} v, \quad \mathbf{x} = \begin{bmatrix} \mathbf{x}_K \\ \mathbf{x}_D \\ \mathbf{x}_S \end{bmatrix} \quad (10)$$

where

$$\mathbf{A} = \begin{bmatrix} \mathbf{A}_{KK} & \mathbf{A}_{K,DS} \\ [0] & \mathbf{A}_{DD} & \mathbf{A}_{DS} \\ [0] & [0] & \mathbf{A}_S \end{bmatrix}, \quad \mathbf{B} = \begin{bmatrix} [0] \\ [0] \\ \mathbf{B}_S \end{bmatrix} \quad (11)$$

$$\mathbf{C} = \begin{bmatrix} \mathbf{C}_K \\ - \\ [0] \\ [0] \end{bmatrix}$$

Remark 1. In its general form, Eq. (10) is time varying. For the simplicity of presentation, the time dependency is not explicitly written.

3. Autopilot-guidance design

In this section, the FS-SL and FS-TL guidance laws are provided. These guidance laws are derived by using the linear equations of motion presented in Section 2.3 and assuming perfect information of the states. The FS-SL and FS-TL designs are presented in Section 3.1 and in Section 3.2, respectively.

3.1. Full-state single-loop guidance law

The FS-SL optimization problem is described in Fig. 2 and given as follows

$$\min_{\mathbf{u}_S} \max_v J = \mathbf{x}^T(t_f) \mathbf{Q}_f \mathbf{x}(t_f) + \int_{t_0}^{t_f} (\mathbf{u}_S^T \mathbf{R} \mathbf{u}_S + \mathbf{x}^T \mathbf{Q} \mathbf{x} - E v^2) d\tau \quad (12)$$

$$\text{s.t. } \dot{\mathbf{x}} = \mathbf{A}_{SL} \mathbf{x} + \mathbf{B}_{SL} \mathbf{u}_S + \mathbf{C} v$$

where the subscript *SL* denotes the FS-SL optimization problem, and t_0 and t_f are the initial and final times, respectively. In this case, the G&C system is designed in a single-loop, thus the open-loop equations of motion are used (Eqs. (10)–(11)), where $\mathbf{A}_{SL} = \mathbf{A}$ and $\mathbf{B}_{SL} = \mathbf{B}$. \mathbf{Q}_f and \mathbf{Q} are real symmetric positive semi-definite matrices; \mathbf{R} is a real symmetric positive definite matrix, and E is a positive scalar. The target

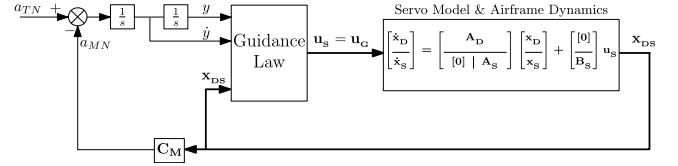


Fig. 2. Block diagram of a full-state single-loop guidance law.

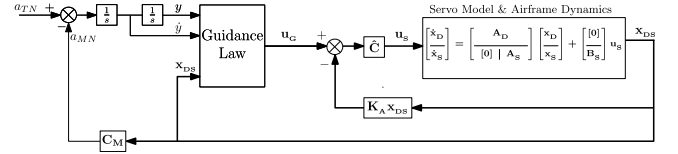


Fig. 3. Block diagram of a full-state two-loop guidance law.

acceleration command v is given by an LQDG guidance law or any other scalar law (constant, step etc.).

The missile and target optimal controllers are (Ho et al., 1965)

$$\mathbf{u}_G^* = \mathbf{u}_S^* = -\mathbf{R}^{-1} \mathbf{B}_{SL}^T \mathbf{P} \mathbf{x} \quad (13)$$

$$v^* = E^{-1} \mathbf{C}^T \mathbf{P} \mathbf{x} \quad (14)$$

where \mathbf{P} is the solution of the differential Riccati equation

$$-\dot{\mathbf{P}} = \mathbf{P} \mathbf{A}_{SL} + \mathbf{A}_{SL}^T \mathbf{P} - \mathbf{P} \mathbf{B}_{SL} \mathbf{R}^{-1} \mathbf{B}_{SL}^T \mathbf{P} + E^{-1} \mathbf{P} \mathbf{C} \mathbf{C}^T \mathbf{P} + \mathbf{Q} \quad (15)$$

with the terminal boundary condition $\mathbf{P}(t_f) = \mathbf{Q}_f$.

3.2. Full-state two-loop autopilot guidance law

The architecture of a FS-TL autopilot guidance law is depicted in Fig. 3. In this case, the inner autopilot loop is designed separately of the outer guidance one, but the guidance law uses information of the entire state vector (kinematics & dynamics states). \mathbf{K}_A denotes the autopilot gain matrix that can be expressed as follows

$$\mathbf{K}_A = [\mathbf{k}_D \quad \mathbf{k}_S], \quad \mathbf{k}_D \in \mathbb{R}^{m_G \times n_D}, \quad \mathbf{k}_S \in \mathbb{R}^{m_G \times n_S} \quad (16)$$

Let $\hat{c} \in \mathbb{R}^{m_S \times m_G}$, then the servo command is given as a function of the states and guidance command

$$\mathbf{u}_S = \hat{c} (\mathbf{u}_G - \mathbf{K}_A \mathbf{x}_{DS}) = \hat{c} \left(\mathbf{u}_G - [\mathbf{k}_D \quad \mathbf{k}_S] \begin{bmatrix} \mathbf{x}_D \\ \mathbf{x}_S \end{bmatrix} \right) \quad (17)$$

The equations of motion with respect to the servo command (open-loop equations) are identical to the FS-SL case

$$\dot{\mathbf{x}} = \mathbf{A}_{SL} \mathbf{x} + \mathbf{B}_{SL} \mathbf{u}_S + \mathbf{C} v \quad (18)$$

Then, by substituting Eq. (17) into Eq. (18), the closed-loop equations of motion are obtained

$$\dot{\mathbf{x}} = \mathbf{A}_{TL} \mathbf{x} + \mathbf{B}_{TL} \mathbf{u}_G + \mathbf{C} v \quad (19)$$

where the subscript *TL* denotes the FS-TL optimization problem, and \mathbf{A}_{TL} and \mathbf{B}_{TL} are given by

$$\mathbf{A}_{TL} = \begin{bmatrix} \mathbf{A}_{KK} & \mathbf{A}_{K,DS} \\ [0] & \mathbf{A}_{DD} & \mathbf{A}_{DS} \\ [0] & -\mathbf{B}_S \hat{c} \mathbf{k}_D & \mathbf{A}_S - \mathbf{B}_S \hat{c} \mathbf{k}_S \end{bmatrix} \quad (20)$$

$$\mathbf{B}_{TL} = \begin{bmatrix} [0] \\ - \\ [0] \\ \mathbf{B}_S \hat{c} \end{bmatrix}$$

To enable a fair comparison between the FS-SL and FS-TL guidance laws, it is assumed that the cost functions of both optimization problems are identical with respect to the servo command. Then, by substituting Eq. (17) into the FS-SL cost function (Eq. (12)), the following FS-TL optimization problem is obtained

$$\min_{\mathbf{u}_G} \max_v J = \mathbf{x}^T(t_f) \mathbf{Q}_f \mathbf{x}(t_f) + \int_{t_0}^{t_f} (\mathbf{u}_G^T \mathbf{R}_{TL} \mathbf{u}_G + 2\mathbf{x}^T \mathbf{S}_{TL} \mathbf{u}_G + \mathbf{x}^T (\mathbf{Q}_{TL} + \mathbf{Q}) \mathbf{x} - E v^2) dt \quad (21)$$

$$\text{s.t. } \dot{\mathbf{x}} = \mathbf{A}_{TL} \mathbf{x} + \mathbf{B}_{TL} \mathbf{u}_G + \mathbf{C} v$$

where

$$\mathbf{R}_{TL} = \hat{\mathbf{C}}^T \mathbf{R} \hat{\mathbf{C}}, \quad \mathbf{S}_{TL} = - \begin{bmatrix} [0] \\ \mathbf{K}_A^T \end{bmatrix} \mathbf{R}_{TL} \quad (22)$$

$$\mathbf{Q}_{TL} = \begin{bmatrix} [0] \\ \mathbf{K}_A^T \end{bmatrix} \mathbf{R}_{TL} \begin{bmatrix} [0] & \mathbf{K}_A \end{bmatrix}$$

Anderson and Moore (1989) introduced the solution of the extended regulator problem, where the performance index contains cross-product terms. Following this solution for the current LQDG problem, an equivalent controller is defined as follows

$$\mathbf{u}_e = \mathbf{u}_G + \mathbf{R}_{TL}^{-1} \mathbf{S}_{TL}^T \mathbf{x} \quad (23)$$

Substituting Eq. (23) into the FS-TL optimization problem (Eq. (21)) and defining

$$\mathbf{A}_e \triangleq \mathbf{A}_{TL} - \mathbf{B}_{TL} \mathbf{R}_{TL}^{-1} \mathbf{S}_{TL}^T \quad (24)$$

$$\mathbf{Q}_e \triangleq \mathbf{Q}_{TL} + \mathbf{Q} - \mathbf{S}_{TL} \mathbf{R}_{TL}^{-1} \mathbf{S}_{TL}^T$$

Then, the equivalent LQDG problem is formulated as follows

$$\min_{\mathbf{u}_e} \max_v J = \mathbf{x}^T(t_f) \mathbf{Q}_f \mathbf{x}(t_f) + \int_{t_0}^{t_f} (\mathbf{u}_e^T \mathbf{R}_{TL} \mathbf{u}_e + \mathbf{x}^T \mathbf{Q}_e \mathbf{x} - E v^2) dt \quad (25)$$

$$\text{s.t. } \dot{\mathbf{x}} = \mathbf{A}_e \mathbf{x} + \mathbf{B}_{TL} \mathbf{u}_e + \mathbf{C} v \quad (26)$$

Now, the equivalent problem can be solved with \mathbf{R}_{TL} being positive definite and \mathbf{Q}_e being nonnegative definite. The missile and target optimal controllers are

$$\mathbf{u}_e^* = -\mathbf{R}_{TL}^{-1} \mathbf{B}_{TL}^T \mathbf{P} \mathbf{x} \quad (27)$$

$$v^* = E^{-1} \mathbf{C}^T \mathbf{P} \mathbf{x} \quad (28)$$

where the differential Riccati equation is

$$-\dot{\mathbf{P}} = \mathbf{P} \mathbf{A}_e + \mathbf{A}_e^T \mathbf{P} - \mathbf{P} \mathbf{B}_{TL} \mathbf{R}_{TL}^{-1} \mathbf{B}_{TL}^T \mathbf{P} + E^{-1} \mathbf{P} \mathbf{C} \mathbf{C}^T \mathbf{P} + \mathbf{Q}_e \quad (29)$$

with the terminal boundary condition $\mathbf{P}(t_f) = \mathbf{Q}_f$.

Let us verify that \mathbf{Q}_e is nonnegative definite by substituting the weights in Eq. (22) into \mathbf{Q}_e (Eq. (24))

$$\mathbf{Q}_e = \mathbf{Q}_{TL} + \mathbf{Q} - \mathbf{S}_{TL} \mathbf{R}_{TL}^{-1} \mathbf{S}_{TL}^T = \mathbf{Q} \quad (30)$$

4. Full-state guidance laws equivalence

This section provides theoretical results concerning the equivalence of the two full-state guidance laws: FS-SL (Section 3.1) and FS-TL (Section 3.2).

Theorem 1. *The necessary and sufficient condition for obtaining identical solutions to the optimization problems of the full-state single-loop case (Eq. (12)) and of the full-state two-loop case (Eq. (21)) is that $\hat{\mathbf{C}}$ is nonsingular.*

Proof. Following the details of the proof given in Levy et al. (2015), Theorem 1 can be easily proven, since the target control effort and the running cost state terms are identical for both the single-loop and two-loop cases.

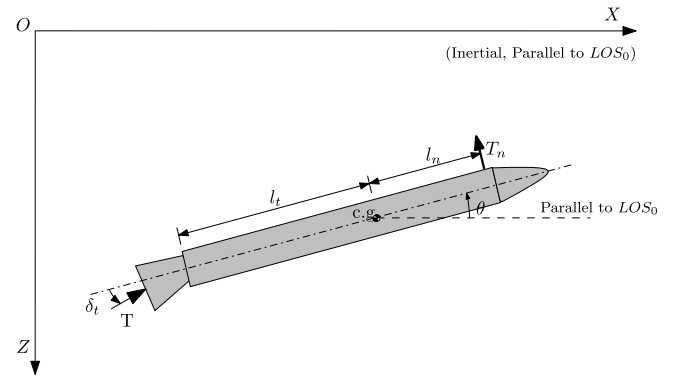


Fig. 4. Basic configuration of a dual-control missile.

5. Test case

In this paper, the guidance laws performance and theorem are demonstrated using a dual-control missile in an exo-atmospheric interception scenario. It should be noted that the end-game scenario is restricted to head-on aerial interception geometries. In the latter, a linear set of equations can be obtained under the assumption of small angles. Two possible autopilot block diagrams are presented based on the number of inputs to the autopilot. These autopilots are used in the FS-TL guidance law, solely. The linearized dual-control missile model is presented next, followed by the autopilot designs.

5.1. Dynamics model

The chosen test case is a dual-control exo-atmospheric missile where a nose jet device was added to a thrust vector control (TVC) missile (Levy et al., 2015). The basic configuration of a dual controlled exo-atmospheric² missile is depicted in Fig. 4. The missile has two controllers, a thrust vector controller as well as a nose jet one. Let θ and δ_t denote the missile's body angle and its thrust deflection (tail controller), respectively. T is the thrust force and l_t is the distance from the center of mass to the nozzle. Let T_n and l_n denote the nose jet force and the distance from the center of mass to the nose jet, respectively.

Assuming first order servo model for both the nose and tail controllers, the state-space formulation of the dynamics model is given as follows

$$\dot{\mathbf{x}}_{DS} = \mathbf{A}_M \mathbf{x}_{DS} + \mathbf{B}_M \mathbf{u}_S \quad (31)$$

$$\mathbf{x}_{DS} = [\theta \quad \dot{\theta} \quad \delta_n \quad \delta_t]^T, \quad \mathbf{u}_S = [\delta_n^c \quad \delta_t^c]^T$$

where δ_n^c and δ_t^c are the deflection commands of the nose jet and the thrust, respectively, and the model matrices

$$\mathbf{A}_M = \begin{bmatrix} \mathbf{A}_D \\ [0] \mid \mathbf{A}_S \end{bmatrix}, \quad \mathbf{A}_D = \begin{bmatrix} 0 & 1 & 0 & 0 \\ 0 & 0 & M \delta_n & -M \delta_t \end{bmatrix} \quad (32)$$

$$\mathbf{A}_S = \begin{bmatrix} -\frac{1}{\tau_n} & 0 \\ 0 & -\frac{1}{\tau_t} \end{bmatrix}, \quad \mathbf{B}_M = \begin{bmatrix} [0] \\ \mathbf{B}_S \end{bmatrix}, \quad \mathbf{B}_S = \begin{bmatrix} \frac{1}{\tau_n} & 0 \\ 0 & \frac{1}{\tau_t} \end{bmatrix}$$

Denote the missile's mass by m , then the thrust component perpendicular to the initial LOS is given by

$$a_{MN} = \mathbf{C}_M \mathbf{x}_{DS}, \quad \mathbf{C}_M = \frac{T}{m} [1 \quad 0 \quad 1 \quad 1] \quad (33)$$

The parameters of the missile and servo are given as follows: $\tau_{n/t} = 0.1$ [s], $T/m = 200$ [m/s²], $M_{\delta_{n/t}} = 330$ [1/s²].

² Outside the atmosphere, the atmospheric density is sufficiently low, therefore the aerodynamic forces and wind can be neglected.

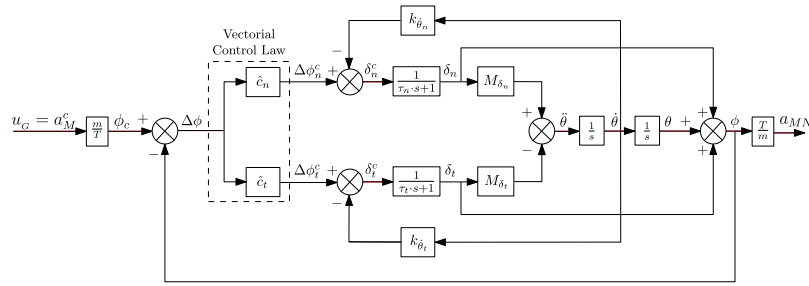


Fig. 5. Single-input autopilot block diagram.

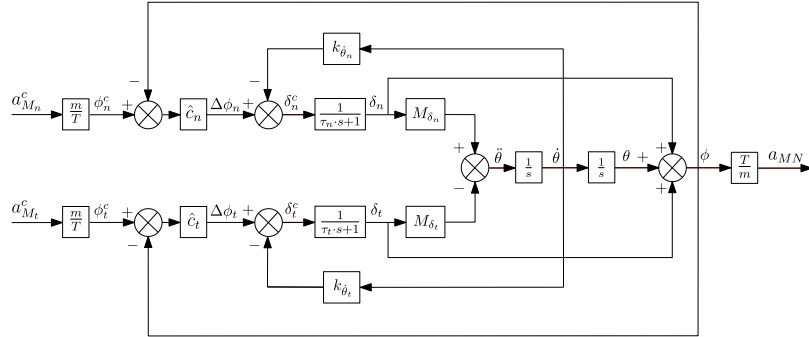


Fig. 6. Multi-input autopilot block diagram.

Remark 2. In a TVC missile, the speed, mass, and inertia are time varying. However, in exo atmospheric scenarios, the speed change is negligible with respect to the total speed. In addition, the guidance law is designed for the end-game phase which is sufficiently short, thus the missile’s speed can be assumed to be nearly constant. This assumption was relaxed in the nonlinear two-dimensional simulation of the missile’s lateral dynamics and relative kinematics presented in Section 8.4.

5.2. Autopilot design

Following Levy et al. (2015), two types of autopilot block diagrams are considered: traditional single-input diagram, and multi-input diagram.

Fig. 5 presents the single-input autopilot diagram. In this case, the guidance command is scalar and the servo command is given by

$$u_s = -K_A x_{DS} + D_u u_G \tag{34}$$

where

$$D_u = \frac{m}{T} \begin{bmatrix} \hat{c}_n \\ \hat{c}_t \end{bmatrix}, \quad K_A = \begin{bmatrix} \hat{c}_n & k_{\theta_n} & \hat{c}_n & \hat{c}_n \\ \hat{c}_t & k_{\theta_t} & \hat{c}_t & \hat{c}_t \end{bmatrix} \tag{35}$$

The autopilot gains are given as follows: $k_{\theta_n} = 0.021$, $k_{\theta_t} = -0.025$, $\hat{c}_n = 0.01$, and $\hat{c}_t = 1$.

The closed-loop autopilot equation is obtained by substituting Eq. (34) into the linearized dynamics in Eqs. (31)–(32)

$$\dot{x}_{DS} = A_{M_{cl}} x_{DS} + B_{M_{cl}} u_G \tag{36}$$

where

$$A_{M_{cl}} = A_M - B_M K_A, \quad B_{M_{cl}} = B_M D_u \tag{37}$$

Fig. 6 presents the multi-input autopilot diagram, where there are two guidance commands that match the number of available controllers. In this way, the guidance law can control each controller individually, resulting in two degrees of freedom. This kind of diagram is tailored for the dual control configuration and therefore may provide the optimal combination of controls for the end-game scenario (Shima & Golan,

2007). The autopilot gains are given as follows: $k_{\theta_n} = 0.021$, $k_{\theta_t} = -0.025$, $\hat{c}_n = 0.0597$, $\hat{c}_t = -0.1126$.

In this case, the servo command is given by

$$u_s = -K_A x_{DS} + D_u u_G \tag{38}$$

where the gains matrix K_A is given in Eq. (35) and D_u is

$$D_u = \frac{m}{T} \begin{bmatrix} \hat{c}_n & 0 \\ 0 & \hat{c}_t \end{bmatrix} \tag{39}$$

By substituting Eq. (38) into the linearized dynamics in Eqs. (31)–(32), the closed-loop autopilot equation is obtained

$$\dot{x}_{DS} = A_{M_{cl}} x_{DS} + B_{M_{cl}} u_G \tag{40}$$

where

$$A_{M_{cl}} = A_M - B_M K_A, \quad B_{M_{cl}} = B_M D_u \tag{41}$$

6. Full-state guidance formulation

The general formulations of the FS-SL and FS-TL guidance laws were presented in Section 3. These formulations will be applied to the dual-control missile test case presented in the previous section.

6.1. Full-state single-loop formulation

Recall the FS-SL formulation provided in Section 3.1

$$\min_{u_s} \max_v J = x^T(t_f) Q_f x(t_f) + \int_{t_0}^{t_f} (u_s^T R u_s + x^T Q x - E v^2) d\tau \tag{42}$$

$$\text{s.t. } \dot{x} = A_{SL} x + B_{SL} u_s + C v \tag{43}$$

This formulation will be applied to the dual-control missile case. The state vector and controller are

$$x = [y \quad \dot{y} \quad \theta \quad \dot{\theta} \quad \delta_n \quad \delta_t]^T, \quad u_s = u_G = [\delta_n^c \quad \delta_t^c]^T \tag{44}$$

and the matrices \mathbf{A}_{SL} and \mathbf{B}_{SL} are

$$\mathbf{A}_{\text{SL}} = \begin{bmatrix} \mathbf{A}_{11} & \mathbf{A}_{12} \\ \mathbf{0} & \mathbf{A}_{22} \end{bmatrix}, \quad \mathbf{A}_{11} = \mathbf{A}_{\text{KK}}, \quad \mathbf{A}_{12} = \mathbf{A}_{\text{K,DS}} \quad (45)$$

$$\mathbf{A}_{22} = \mathbf{A}_{\text{M}}, \quad \mathbf{B}_{\text{SL}} = \begin{bmatrix} \mathbf{0} \\ \mathbf{B}_{\text{M}} \end{bmatrix}$$

where \mathbf{A}_{M} and \mathbf{B}_{M} are given in Eq. (32), the matrices \mathbf{A}_{KK} and $\mathbf{A}_{\text{K,DS}}$ are given in Eq. (9), and the vector \mathbf{C} is given in Eq. (11).

The chosen weight matrices

$$\mathbf{R} = \begin{bmatrix} d^2 & 0 \\ 0 & 1 \end{bmatrix}, \quad \mathbf{Q}_{\text{r}}(i, j) = \begin{cases} c^2, & \text{if } i = j = 1 \\ 0, & \text{else} \end{cases} \quad (46)$$

$$\mathbf{Q}(i, j) = \begin{cases} b^2, & \text{if } i = j = 3 \\ 0, & \text{else} \end{cases}$$

where $1 \leq i, j \leq 6$, d is the nose control effort penalty, c is the miss distance penalty, and b is the attitude angle penalty. The target control effort penalty is set as follows: $E = e^2$.

6.2. Full-state two-loop formulation

Recall that in this case, there is an inner autopilot loop, thus the servo command is determined by the autopilot diagram and is a function of the guidance command and states. Two types of autopilot block diagram were presented in the previous section: single-input diagram (Fig. 5) and multi-input diagram (Fig. 6). The FS-TL guidance law will be formulated for both autopilot diagrams, where the chosen weight matrices are identical to the FS-SL weight matrices in Eq. (46) to enable future comparison between the two guidance laws.

6.2.1. Single-input autopilot

By using the single-input autopilot diagram (Fig. 5), the guidance law issues a single command, which is divided into two equivalent commands by a vectorial control law. The corresponding FS-TL optimization problem is obtained by substituting the servo command from Eq. (34) into the FS-SL optimization problem (Eqs. (42)–(43))

$$\min_{\mathbf{u}_{\text{G}}} \max_v J = \mathbf{x}^T(t_f) \mathbf{Q}_{\text{f}} \mathbf{x}(t_f) + \int_{t_0}^{t_f} (\mathbf{D}_{\text{u}}^T \mathbf{R} \mathbf{D}_{\text{u}} \mathbf{u}_{\text{G}}^2 + 2\mathbf{x}^T \mathbf{C}_{\text{u}}^T \mathbf{R} \mathbf{D}_{\text{u}} \mathbf{u}_{\text{G}} + \mathbf{x}^T \mathbf{C}_{\text{u}}^T \mathbf{R} \mathbf{C}_{\text{u}} \mathbf{x} + \mathbf{x}^T \mathbf{Q} \mathbf{x} - E v^2) dt \quad (47)$$

$$\text{s.t. } \dot{\mathbf{x}} = \mathbf{A}_{\text{TL}} \mathbf{x} + \mathbf{B}_{\text{TL}} \mathbf{u}_{\text{G}} + \mathbf{C} v \quad (48)$$

where $\mathbf{C}_{\text{u}} = \begin{bmatrix} \mathbf{0} & -\mathbf{K}_{\text{A}} \end{bmatrix}$ and the matrices \mathbf{A}_{TL} and \mathbf{B}_{TL} are given as follows

$$\mathbf{A}_{\text{TL}} = \begin{bmatrix} \mathbf{A}_{11} & \mathbf{A}_{12} \\ \mathbf{0} & \mathbf{A}_{\text{M}_{\text{cl}}} \end{bmatrix}, \quad \mathbf{B}_{\text{TL}} = \begin{bmatrix} \mathbf{0} \\ \mathbf{B}_{\text{M}_{\text{cl}}} \end{bmatrix} \quad (49)$$

The matrices $\mathbf{A}_{\text{M}_{\text{cl}}}$ and $\mathbf{B}_{\text{M}_{\text{cl}}}$ are given in Eqs. (36)–(37).

6.2.2. Multi-input autopilot

By using the multi-input autopilot diagram (Fig. 6), the guidance command is a two-dimensional vector $\mathbf{u}_{\text{G}} = \begin{bmatrix} a_{M_n}^c & a_{M_t}^c \end{bmatrix}^T$. The corresponding FS-TL optimization problem is obtained by substituting the servo command from Eq. (38) into the FS-SL optimization problem (Eqs. (42)–(43))

$$\min_{\mathbf{u}_{\text{G}}} \max_v J = \mathbf{x}^T(t_f) \mathbf{Q}_{\text{f}} \mathbf{x}(t_f) + \int_{t_0}^{t_f} (\mathbf{u}_{\text{G}}^T \mathbf{D}_{\text{u}}^T \mathbf{R} \mathbf{D}_{\text{u}} \mathbf{u}_{\text{G}} + 2\mathbf{x}^T \mathbf{C}_{\text{u}}^T \mathbf{R} \mathbf{D}_{\text{u}} \mathbf{u}_{\text{G}} + \mathbf{x}^T \mathbf{C}_{\text{u}}^T \mathbf{R} \mathbf{C}_{\text{u}} \mathbf{x} + \mathbf{x}^T \mathbf{Q} \mathbf{x} - E v^2) dt \quad (50)$$

$$\text{s.t. } \dot{\mathbf{x}} = \mathbf{A}_{\text{TL}} \mathbf{x} + \mathbf{B}_{\text{TL}} \mathbf{u}_{\text{G}} + \mathbf{C} v \quad (51)$$

where the forms of \mathbf{A}_{TL} and \mathbf{B}_{TL} are identical to the ones in Eq. (49), and the matrices $\mathbf{A}_{\text{M}_{\text{cl}}}$ and $\mathbf{B}_{\text{M}_{\text{cl}}}$ are given in Eqs. (40)–(41).

7. Target evasion strategies

The full-state guidance laws performance analysis will be examined against two types of target evasion strategies: (1) Linear controller based on the LQDG solution; (2) “Bang–Bang” controller based on the optimal evasion solution.

7.1. Linear controller — LQDG based

The LQDG evasion strategy for the FS-SL and FS-TL guidance laws is given in Sections 3.1 and 3.2, respectively. However, for the sake of consistency it is presented here also

$$\mathbf{v}^* = \mathbf{E}^{-1} \mathbf{C}^T \mathbf{P} \mathbf{x} \quad (52)$$

where \mathbf{P} is the solution of the corresponding Riccati equation in the FS-SL case (Eq. (15)) or in the FS-TL case (Eq. (29)).

It can be seen that Eq. (52) is a linear evasion strategy. The latter originates from the conventional LQDG formulation, where the cost function is composed of three quadratic terms: miss distance squared, and the control energy integrals of both the evader and the pursuer (Turetsky & Shinar, 2003). Such a formulation generates linear strategies (“soft” controls) for both players. These strategies are easy to implement, but may not be adopted by both players since the LQDG cost represents a compromise between different objectives rather than the guaranteed miss distance. Furthermore, the LQDG evasion strategy is proportional to the entire state vector, including the relative displacement. The latter implies that when both players are on a collision course, the target will issue no command. Therefore, the LQDG evasion strategy might not be suitable to represent a realistic evading strategy as shown in Section 8.2.

7.2. “Bang–Bang” controller — optimal control based

The optimal evasion strategy against an LQDG guided missile is obtained by substituting the missile’s guidance command into the equations of motion. The FS-SL and FS-TL guidance commands are given in Eq. (13) and Eqs. (23), (27), respectively. These commands can be represented by the following feedback law

$$\mathbf{u}^* = \mathbf{N}^*(t_{go}) \mathbf{x} \quad (53)$$

Substituting Eq. (53) into the appropriate equation of motion and taking the absolute value of the miss-distance as the payoff, the following optimal control problem can be formulated

$$\max_v J = |y(t_f)| \quad (54)$$

$$\text{s.t. } \dot{\mathbf{x}} = \mathbf{A}_{\text{CL}}(t_{go}) \mathbf{x} + \mathbf{C} v \quad (55)$$

$$|v| \leq \rho_v \quad (56)$$

where \mathbf{A}_{CL} is the closed loop matrix and ρ_v is the target acceleration bound. Denote the adjoint vector by $\lambda_{\mathbf{x}}$, then the Hamiltonian is

$$H = \lambda_{\mathbf{x}}^T (\mathbf{A}_{\text{CL}}(t_{go}) \mathbf{x} + \mathbf{C} v) \quad (57)$$

The adjoint variable has to satisfy the following Euler–Lagrange equation

$$\dot{\lambda}_{\mathbf{x}} = -\frac{\partial H}{\partial \mathbf{x}} = -\mathbf{A}_{\text{CL}}^T(t_{go}) \lambda_{\mathbf{x}} \quad (58)$$

and the transversality condition

$$\lambda_{\mathbf{x}}(t_f) = \frac{\partial J}{\partial \mathbf{x}} \Big|_{t_f} = [\text{sign } y(t_f) \quad \mathbf{0}^{1 \times 5}]^T \quad (59)$$

Candidate optimal strategies are obtained by direct minimization of the Hamiltonian in Eq. (57)

$$\mathbf{v}^* = \rho_v \text{sign}(\lambda_{\mathbf{x}}^T \mathbf{C}) \quad (60)$$

The optimal strategy in Eq. (60) is of “bang–bang” type. It is noteworthy that the optimal evasion strategy against a proportional navigation guided missile, while considering a bounded target command, has also a “bang–bang” structure (Gutman & Goldan, 2009; Shinar & Steinberg, 1977). It is shown in Section 8.3 that such nonlinear evasion strategy generates a non-zero miss-distance against an LQDG guided missile.

8. Simulation results

In this section, the performance of the two full-state guidance laws (FS-SL and FS-TL) is exemplified using the dual-control missile model (Section 5.1) in linear and nonlinear settings. Simulations were made for two types of target acceleration commands: (1) LQDG based linear controller (Eq. (52)); (2) Optimal “bang–bang” controller (Eq. (60)).

The FS-SL optimization problem formulation is specified in Section 6.1. The FS-TL optimization problem has a different formulation for each of the autopilot diagrams: single-input diagram and multi-input diagram. The FS-TL single-input case is denoted by FS-TL (SI), where its formulation is given in Section 6.2.1. The FS-TL multi-input case is denoted by FS-TL (MI), where its formulation is given in Section 6.2.2.

First, the linear and nonlinear test scenarios are outlined in Section 8.1. Then, the performance of the guidance laws is analyzed using the linear test case for each of the target strategies in Sections 8.2–8.3. Finally, nonlinear simulation results are presented in Section 8.4.

8.1. Linear and nonlinear test scenarios

The performance of the guidance laws is evaluated using linear and nonlinear test scenarios.

The linear test case is used for demonstrating the guidance laws performance against the two types of target acceleration commands. In this setting, the next initial conditions are used: $y_0 = 200$ [m], $\dot{y}_0 = 0$ [m/s], $\theta_0 = \delta_{n0} = \delta_{i0} = 0$ [deg], $\dot{\theta}_0 = 0$ [deg/s]. It can be seen that the scenarios are initiated close to the collision course, following the design assumptions (see Section 2.1).

The nonlinear test case is used for investigating and comparing the FS-SL and FS-TL guidance laws performance in a more realistic setting. In this setting, a nonlinear two-dimensional simulation of the missile’s lateral dynamics and relative kinematics is used, where the target applies the optimal “bang–bang” evasion strategy against the LQDG guided missile. Such an evasion strategy will be shown to be more suitable to represent the target maneuver than the LQDG one. The initial conditions are given as follows: $r_0 = 9000$ [m], $V_{M0} = V_{T0} = 1500$ [m/s], $\gamma_{M0} = 0$ [deg], $\gamma_{T0} = 2$ [deg], $\lambda_0 = 2$ [deg], $\theta_0 = \delta_{n0} = \delta_{i0} = 0$ [deg], $\dot{\theta}_0 = 0$ [deg/s].

Remark 3. It is noteworthy that in the nonlinear case, the final time was obtained iteratively. At each iteration, the final time was updated with the current range and range rate and the Riccati equations were recalculated for the updated final time.

8.2. LQDG based target maneuver

In this case, both adversaries use an LQDG guidance law, and the penalties on the attitude angle and nose control effort are fixed: $b = 0.3$, and $d = 1$. The FS-SL cost function is

$$J = c^2 y^2(t_f) + \int_{t_0}^{t_f} \{d^2 \delta_n^2 + \delta_i^2 + b^2 \theta^2 - e^2 v^2\} d\tau \quad (61)$$

In Ho et al. (1965) and Ben-Asher and Yaesh (1998) it was shown that the existence of a solution to the corresponding Riccati equation (the nonexistence of a conjugate point) is a sufficient condition for the existence of a saddle point solution. The Riccati Eqs. of the FS-SL and FS-TL guidance laws are given in Eq. (15) and Eq. (29), respectively. Fig. 7 presents the boundary curves of both full-state guidance laws as a function of the penalties c and e . A conjugate point does not exist to the

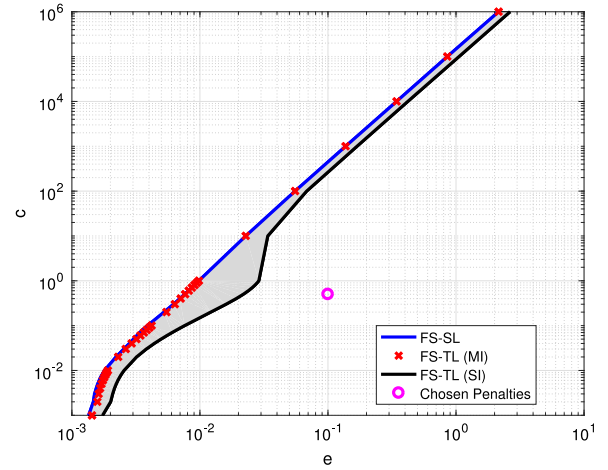


Fig. 7. Conjugate point conditions (LQDG target maneuver, linear simulation).

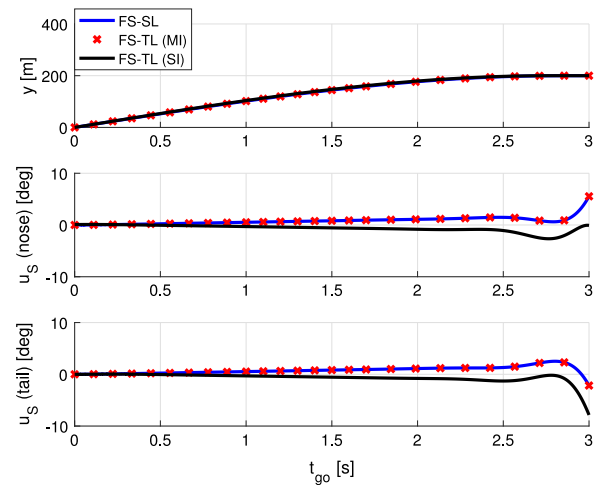


Fig. 8. Relative displacement and servo commands (LQDG target maneuver, linear simulation).

right of each boundary curve. It can be seen that the curves of the FS-SL and of the FS-TL (MI) overlap. The curve of the FS-TL (SI) appears to the right of the FS-SL curve, thus implying that for a given miss distance penalty (c), a less maneuverable target is allowed (larger e). The gray area indicates the additional area of allowed penalties offered by using FS-SL, or equivalently using FS-TL (MI).

Figs. 8–9 present the results of the FS-SL and FS-TL guidance laws for the following penalties: $e = 0.1$, $c = 0.5$ (see the purple circle in Fig. 7). It can be seen that the results of the FS-SL case and FS-TL (MI) overlap, as expected. The attitude angle is kept within its physical domain (Fig. 9) due to the addition of an appropriate running cost term to the cost function. Furthermore, it is apparent that the miss distance is approximately zero $y(t_f) \sim 0$ and the target hardly maneuvers throughout the entire scenario. It is obvious that a rational target will try to maximize the miss distance rather than stay on a collision course till interception and therefore will not adopt the LQDG strategy. To emphasize this point, the optimal evasion strategy against an LQDG maneuvering missile is derived in the next section.

8.3. Optimal “Bang–Bang” evasion strategy

In this section, the optimal evasion strategy against an LQDG guided missile while assuming a known target acceleration bound is presented.

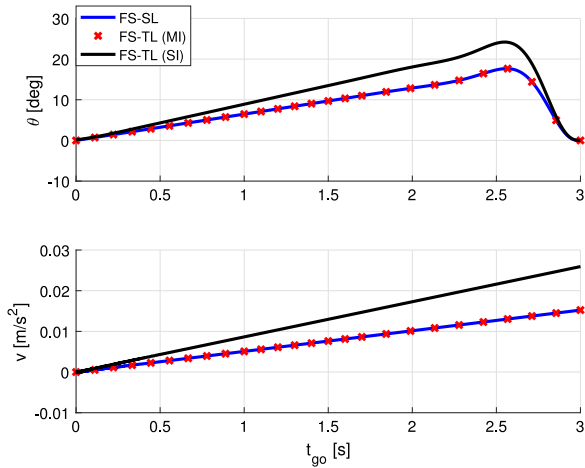


Fig. 9. Attitude angle and target acceleration command (LQDG target maneuver, linear simulation).

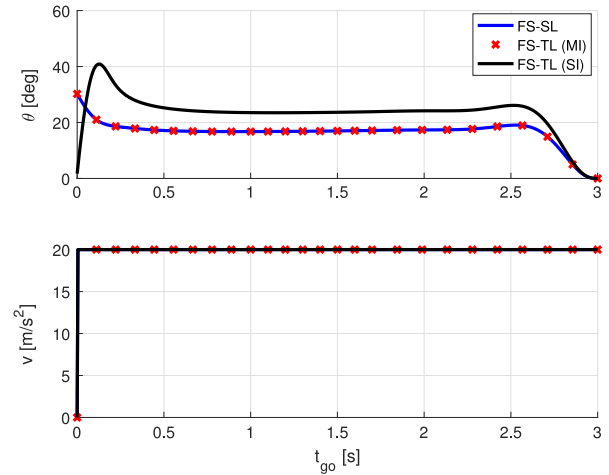


Fig. 11. Attitude angle and target acceleration command (“Bang-Bang” target maneuver, linear simulation).

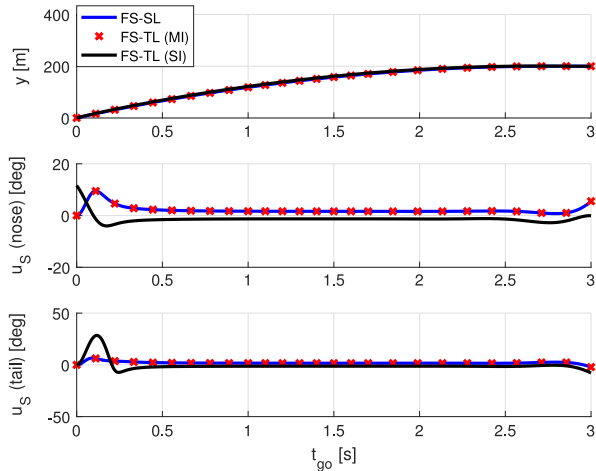


Fig. 10. Relative displacement and servo commands (“Bang-Bang” target maneuver, linear simulation).

It is shown that such a strategy renders non zero miss distance as opposed to the LQDG one. The results are computed for the penalties chosen in the previous section: $b = 0.3$, $d = 1$, $e = 0.1$, and $c = 0.5$

Figs. 10–11 present the results of the full-state guidance laws for a fixed target acceleration bound: $\rho_v = 20$ [m/s²]. It can be seen that the results of the FS-SL and FS-TL(MI) are identical, thus implying their equivalence. In this case, the attitude angle and servo commands were kept at reasonable values due to appropriate penalization in the cost function, where $|\theta(t_{go})| < 31$ [deg] and $|\delta_n^c(t_{go})|, |\delta_t^c(t_{go})| \leq 10$ [deg] $\forall t_{go} \in [0, t_f]$. However by using the FS-TL (SI) architecture, the attitude angle exceeded beyond its physical domain where its maximal value is 41 [deg]. In the FS-SL case (or FS-TL (MI) case), the obtained miss distance is acceptable ($y(t_f) = 0.16$ [m]), whereas in the FS-TL (SI) case, the obtained miss distance is much higher $y(t_f) = 0.45$ [m].

8.4. Nonlinear test case

In this section, the two full-state guidance laws performance is analyzed using a two-dimensional nonlinear simulation of the missile’s lateral dynamics and of the relative kinematics. The missile dynamics and relative kinematics equations are presented in Appendix. In addition, the missile’s servo commands are bounded by $\delta_{max} = 20$ [deg]

as follows

$$|\delta_\chi^c| = \delta_{max}, \quad \chi = \{n, t\} \quad (62)$$

In this case, the target is assumed to apply the optimal evasion strategy against an LQDG guided missile, where its acceleration bound is assumed to be known and equal to 20 [m/s²]. The target’s speed is assumed to be constant throughout the entire scenario. It is noteworthy, that the optimal evasion strategy is calculated separately for each of the three full-state guidance laws, i.e FS-SL, FS-TL(MI), and FS-TL(SI).

The results are obtained for the following penalties: $b = 0.5$, $d = 1$, $c = 0.5$, and $e = 0.1$. The existence of a saddle point solution (the nonexistence of a conjugate point) was verified by checking that the solution of the corresponding Riccati equation exist (see Section 8.2).

Figs. 12–15 present the results of the three different guidance laws: FS-SL, FS-TL(MI), FS-TL(SI). The results of the FS-SL case and FS-TL (MI) overlap, as expected. Therefore, from this point onwards, only the FS-TL(MI) and the FS-TL(SI) guidance laws are discussed.

Fig. 12 presents the trajectories of the missile and target (note the different scaling in the X and Z axis). The missile trajectories are in blue, where the target trajectories are in red. It can be seen that the FS-TL(MI) guided missile reached the target before the FS-TL(SI) guided missile. The miss distance obtained by using FS-TL(MI) is 0.1 [m], where the miss distance obtained in the FS-TL(SI) guidance law is 0.92 [m]. These results imply the superiority of the FS-TL (MI) architecture over the FS-TL (SI) one.

Fig. 13 presents the servo deflections and attitude angle. The FS-TL(MI) servo deflections did not reach saturation throughout the entire scenario. The FS-TL(SI) tail servo deflection reached saturation close to interception at $t_{go} = 0.16$ [s]. The latter had a dramatic influence on the miss distance as it is 9 times bigger than the FS-TL(MI) miss distance. In addition, it can be seen that the attitude angle obtained by using FS-TL(SI) law is much higher than the one obtained by using FS-TL (MI).

The path angles and missile’s speed are presented in Fig. 14. It can be seen that by using an FS-TL(MI) guidance law, the missile’s speed is higher than by using an FS-TL(SI) law. The target’s speed and optimal evasion maneuver are constant (see Fig. 15), hence its path angle variation is linear and identical for all three guidance laws.

9. Conclusions

In this paper, the conditions for obtaining an equivalence relation between the full-state single-loop and the full-state two-loop guidance and control architectures were derived under a linear quadratic differential game formulation. It was proven that the two full-state guidance laws

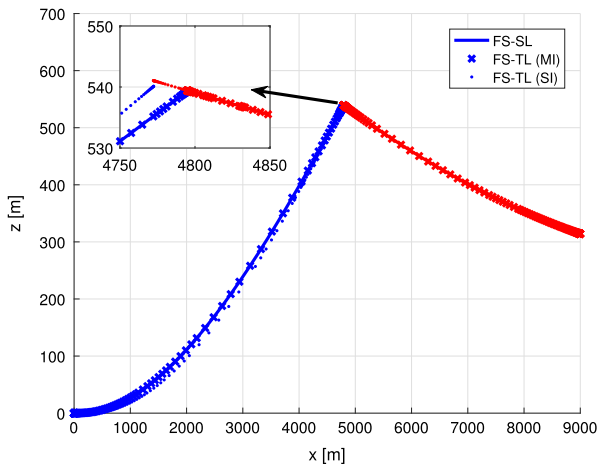


Fig. 12. Missile and target trajectories (nonlinear simulation, missile traj.- blue, target traj.- red). (For interpretation of the references to color in this figure legend, the reader is referred to the web version of this article.)

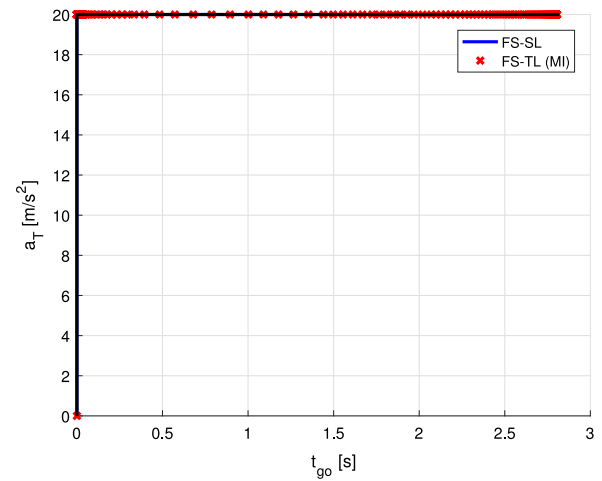


Fig. 15. Target acceleration command (nonlinear simulation).

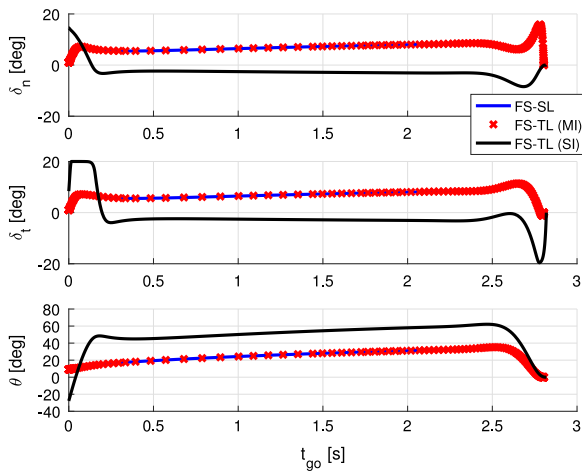


Fig. 13. Servo deflections and attitude angle (nonlinear simulation).

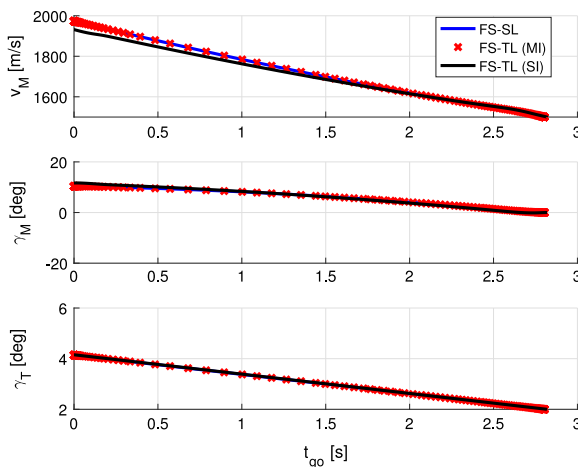


Fig. 14. Missile speed and path angles (nonlinear simulation).

are identical if and only if the number of guidance commands matches to the number of available controllers.

The guidance laws performance was illustrated by using a dual-control missile in an exo-atmospheric scenario in linear and nonlinear settings. Two types of autopilot block diagrams were used in the full-state two-loop case: single-input diagram and a multi-input diagram. In the multi-input diagram, there are two guidance commands that match the number of available controllers, whereas in the single-input diagram, the guidance law issues a single acceleration command. It was shown that by using a multi-input autopilot, the full-state two-loop guidance law was able to achieve the same results as the full-state single-loop guidance law. The advantage of using a multi-input diagram over a single-input one was most noticeable in the nonlinear test case. In this case, the tail servo deflection of the single-input case reached saturation close to interception thus resulting a miss distance increase. In addition, it was shown that the attitude angle may be kept at reasonable values by proper penalization, while still obtaining the required miss distance.

It was shown that it is impractical to use a linear quadratic differential game based evasion strategy represent the target maneuver. Using such a strategy, the target appears to stay on a collision course till interception rather than maximize the miss-distance. As a consequence, the guidance laws performance was investigated for the optimal “bang-bang” evasion maneuver against a linear quadratic differential game maneuvering missile. It was shown that by using such a strategy, non zero miss distance is rendered, and hence it may represent a rational target maneuver.

Acknowledgments

This research was supported by the Israel Science Foundation - grant 1469/15.

Appendix. Nonlinear simulation models

This appendix presents the nonlinear models of the relative kinematics and missile lateral dynamics. These models were used in the nonlinear test case, presented in Section 8.4.

First, the relative kinematics equations are presented, followed by the missile dynamics model

A.1. Nonlinear relative kinematics

A schematic view of the planar end-game geometry is presented in Fig. 1. Let V_r and V_λ denote the speeds along and perpendicular to the

LOS. Then, the kinematics equations³ expressed in a polar coordinate system (r, λ) attached to the missile, are

$$\dot{r} = V_r \quad (\text{A.1})$$

$$\dot{\lambda} = V_\lambda / r \quad (\text{A.2})$$

where

$$V_r = -[V_M \cos(\gamma_M - \lambda) + V_T \cos(\gamma_T + \lambda)] \quad (\text{A.3})$$

$$V_\lambda = -V_M \sin(\gamma_M - \lambda) + V_T \sin(\gamma_T + \lambda) \quad (\text{A.4})$$

The time to go is approximated by the following expression

$$t_{go} = -r/V_r \quad (\text{A.5})$$

During the end-game, the target dynamics is assumed to be ideal to consider a realistic scenario where there is no information on its dynamics. In this manner, by assuming that the target speed is constant during the endgame, the target lateral maneuver is given by

$$\dot{\gamma}_T = \frac{a_T}{v_T} \quad (\text{A.6})$$

where a_T is given by a linear controller based on the LQDG solution or a “bang–bang” controller based on the optimal evasion solution.

A.2. Nonlinear missile lateral dynamics

The basic configuration of a dual-control exo-atmospheric missile is presented in Fig. 4. The planar missile dynamics can be expressed as

$$\dot{V}_M = \frac{T}{m} \cos(\theta + \delta_t - \gamma_M) - \frac{T_n}{m} \sin(\theta - \gamma_M) \quad (\text{A.7})$$

$$\dot{\gamma}_M = \left[\frac{T}{m} \sin(\theta + \delta_t - \gamma_M) + \frac{T_n}{m} \cos(\theta - \gamma_M) \right] / V_M \quad (\text{A.8})$$

$$\dot{\theta} = M_{\delta_n} \delta_n - M_{\delta_t} \sin(\delta_t) \quad (\text{A.9})$$

where $\frac{T_n}{m} \triangleq \frac{T}{m} \delta_n$ and first order servo model is assumed for both the nose and tail controllers

$$\dot{\delta}_\chi = (\delta_\chi^c - \delta_\chi) / \tau_\chi, \quad \chi = \{n, t\} \quad (\text{A.10})$$

References

Anderson, B. D., & Moore, J. B. (1989). *Optimal control, linear quadratic methods*. (pp. 7–67). Englewood Cliffs, New Jersey: Prentice Hall.

Ben-Asher, J. Z., Levinson, S., Shinar, J., & Weiss, H. (2004). Trajectory shaping in linear-quadratic pursuit-evasion games. *AIAA Journal of Guidance, Control, and Dynamics*, 27(6), 1102–1105. <http://dx.doi.org/10.2514/1.9765>.

Ben-Asher, J. Z., & Yaesh, I. (1998). *Advances in missile guidance theory*, (Vol. 180). (pp. 25–88). Reston, Virginia: American Institute of Aeronautics and Astronautics.

Gutman, S., & Goldan, O. (2009). Proportional navigation miss distance in the presence of bounded inputs. *AIAA Journal of Guidance, Control, and Dynamics*, 35(3), 816–823. <http://dx.doi.org/10.2514/1.41713>.

Gutman, S., Rubinsky, S., Shima, T., & Levy, M. (2013). Single vs. Two-loop integrated guidance systems. In *Proceedings of the CEAS euro GNC conference* (pp. 1–15). Delft, The Netherlands.

Ho, Y.-C., Bryson, A., & Baron, S. (1965). Differential games and optimal pursuit-evasion strategies. *IEEE Transactions on Automatic Control*, 10(4), 385–389. <http://dx.doi.org/10.1109/TAC.1965.1098197>.

Idan, M., Shima, T., & Golan, O. M. (2007). Integrated sliding mode autopilot-guidance for dual-control missiles. *AIAA Journal of Guidance, Control, and Dynamics*, 30(4), 1081–1089. <http://dx.doi.org/10.2514/1.24953>.

Isaacs, R. (1965). *Differential games: a mathematical theory with applications to warfare and pursuit, control and optimization*. New York: Wiley.

Levy, M., Shima, T., & Gutman, S. (2013). Linear quadratic integrated vs. Separated autopilot-guidance design. *AIAA Journal of Guidance, Control, and Dynamics*, 36(6), 1722–1730. <http://dx.doi.org/10.2514/1.61363>.

Levy, M., Shima, T., & Gutman, S. (2014). Full-state autopilot-guidance design under a linear quadratic differential game formulation. In *Proceedings of the 19th world congress of the international federation of automatic control* (pp. 3942–3947). Cape Town, South Africa.

Levy, M., Shima, T., & Gutman, S. (2015). Single versus two-loop full-state multi-input missile guidance. *AIAA Journal of Guidance, Control, and Dynamics*, 38(5), 843–853. <http://dx.doi.org/10.2514/1.G000171>.

Levy, M., Shima, T., & Gutman, S. (2017). Single vs. Two-loop full-state guidance and control. *Journal of Guidance, Control, and Dynamics*, 40(8), 1968–1977. <http://dx.doi.org/10.2514/1.G002722>.

Menon, P. K., & Ohlmeyer, E. J. (2001). Integrated design of agile missile guidance and autopilot systems. *Control Engineering Practice*, 9(10), 1095–1106. [http://dx.doi.org/10.1016/S0967-0661\(01\)00082-X](http://dx.doi.org/10.1016/S0967-0661(01)00082-X).

Menon, P. K., Sweriduk, G. D., & Ohlmeyer, E. J. (2003). Optimal fixed-interval integrated guidance-control laws for hit-to-kill missiles. In *AIAA Guidance, Navigation, and Control Conference* (pp. 1–9).

Palumbo, N. F., Reardon, B. E., & Blauwkamp, R. A. (2004). Integrated guidance and control for homing missiles. *Johns Hopkins Apl Technical Digest*, 25(2), 121–139.

Rusnak, I., & Levi, M. (1991). Modern guidance law for high-order autopilot. *AIAA Journal of Guidance, Control, and Dynamics*, 14(5), 1056–1058. <http://dx.doi.org/10.2514/3.20749>.

Shima, T., & Golan, O. M. (2007). Linear quadratic differential games guidance law for dual controlled missiles. *IEEE Transactions on Control Systems Technology*, 43(3), 834–842. <http://dx.doi.org/10.1109/TAES.2007.4383577>.

Shima, T., Idan, M., & Golan, O. M. (2006). Sliding-mode control for integrated missile autopilot guidance. *AIAA Journal of Guidance, Control, and Dynamics*, 29(2), 250–260. <http://dx.doi.org/10.2514/1.14951>.

Shinar, J., & Steinberg, D. (1977). Analysis of optimal evasive maneuvers based on a linearized two-dimensional kinematic model. *Journal of Aircraft*, 14(8), 795–802. <http://dx.doi.org/10.2514/3.58855>.

Shkolnikov, I., Shtessel, Y. B., & Lianos, D. (2001). Integrated guidance-control system of a homing interceptor: sliding mode approach. In *Proceeding of the AIAA guidance, navigation, and control conference* (pp. 1–11). <http://dx.doi.org/10.2514/6.2001-4218>.

Turetsky, V., & Shinar, J. (2003). Missile guidance laws based on pursuit-evasion game formulations. *Automatica*, 39(4), 607–618. [http://dx.doi.org/10.1016/S0005-1098\(02\)00273-X](http://dx.doi.org/10.1016/S0005-1098(02)00273-X).

³ The kinematics equations are derived while neglecting the difference between the gravitational forces of the target and missile.